Farzan, Afsoon; Borandeh, Sedigheh; Zanjanizadeh Ezazi, Nazanin; Lipponen, Sami; Santos, Hélder A.; Seppälä, Jukka

3D scaffolding of fast photocurable polyurethane for soft tissue engineering by stereolithography: Influence of materials and geometry on growth of fibroblast cells

Published in:
European Polymer Journal

DOI:
10.1016/j.eurpolymj.2020.109988

Published: 05/10/2020

Document Version
Peer-reviewed accepted author manuscript, also known as Final accepted manuscript or Post-print

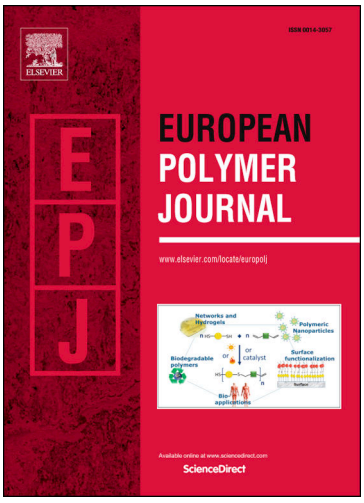

3D Scaffolding of fast photocurable polyurethane for soft tissue engineering by stereolithography: Influence of materials and geometry on growth of fibroblast cells

Afsoon Farzan, Sedigheh Borandeh, Nazanin Zanjanizadeh Ezazi, Sami Lipponen, Hélder A. Santos, Jukka Seppälä

PII: S0014-3057(20)31702-X
DOI: https://doi.org/10.1016/j.eurpolymj.2020.109988
Reference: EPJ 109988

To appear in: *European Polymer Journal*

Received Date: 26 June 2020
Revised Date: 26 August 2020
Accepted Date: 27 August 2020

Please cite this article as: Farzan, A., Borandeh, S., Zanjanizadeh Ezazi, N., Lipponen, S., Santos, H.A., Seppälä, J., 3D Scaffolding of fast photocurable polyurethane for soft tissue engineering by stereolithography: Influence of materials and geometry on growth of fibroblast cells, *European Polymer Journal* (2020), doi: https://doi.org/10.1016/j.eurpolymj.2020.109988

Revised

3D Scaffolding of fast photocurable polyurethane for soft tissue engineering by stereolithography: Influence of materials and geometry on growth of fibroblast cells

Afsoon Farzan[a], Sedigheh Borandeh[a], Nazanin Zanjanizadeh Ezazi[b,c], Sami Lipponen[a], Hélder A. Santos[b,c], Jukka Seppälä[a*]

[a]*Polymer Technology, School of Chemical Engineering, Aalto University, Kemistintie 1, 02150 Espoo, Finland;*

[b]*Drug Research Program, Division of Pharmaceutical Chemistry and Technology, Faculty of Pharmacy, University of Helsinki, FI-00014, Finland;*

[c]*Helsinki Institute of Life Sciences, HiLIFE, University of Helsinki, FI-00014 Finland.*

[*] Corresponding author

Email address: jukka.seppala@aalto.fi (J. Seppälä)

Abstract

Tissue engineering can benefit from the availability of three-dimensional (3D) printing technologies that make it possible to produce scaffolds with complex geometry. Chemical, mechanical, and structural properties should be considered in scaffold design and development since these properties affect cell adhesion, proliferation, and differentiation. To this end, in this study, we developed a series of fast photocuring polyurethanes (PUs), using poly(ε-caprolactone) (PCL) and/or polyethylene glycol (PEG) as microdiols, using a solvent-free method and stereolithography strategy for the fabrication of elastic 3D-printed scaffold. The effects of different diols on the hydrolytic degradation, thermal and mechanical properties, and hydrophilicity of PUs were evaluated. The results showed that PEG-containing PUs had higher degradation rates, and the tensile strength of PU/PCL/PEG was 1.4 and 2 times higher than that of PU/PEG and PU/PCL, respectively. Moreover, the effect of different diols and scaffold geometry on toxicity and cell attachment were studied *in vitro*. The results of MTT and AlamarBlue assays on dermal fibroblast cells showed high proliferation of printed PU/PCL/PEG scaffold with no sign of cytotoxicity. In addition, compared to cast film PUs, relatively high cell attachment was seen on the surface of printed PU/PCL/PEG even after 4 days. Therefore, 3D printed PU/PCL/PEG showed high applicability in soft tissue engineering, especially for scaffold development.

Keywords: 3D printing; Polyurethane; Tissue engineering; Cell attachment; Stereolithography.

1. Introduction

Recently, considerable attention has been paid to the investigation and development of scaffolds for tissue engineering and regenerative medicine. In particular, polymeric biomaterials have been widely studied and used in medical interventions and therapies [1, 2].

In the last two decades, research has focused more on the clinical applications of polymeric biomaterials, especially for tissue engineering and regeneration [3-7]. Using polymers as scaffolds to repair and regenerate damaged tissues often requires specific, individual, and tunable properties. To work in an optimized manner, the utilized polymers should be biocompatible, biodegradable, and have high porosity, together with interconnected/lined pores and adequate mechanical properties. In addition to biocompatibility and mechanical properties, the geometrical structure of the scaffolds should be considered [3, 8-11].

Advances in three-dimensional (3D) printing have enabled the preparation of well-organized and complex scaffolds made by polymeric materials. The 3D-printing technique has especially found applications in biomedical fields, where individual 'spare parts' are needed [12, 13]. Fast fabrication, high precision, and customized production are some advantages of using 3D-printing techniques in biomedical applications [14-17]. 3D-printed scaffolds for tissue engineering can be prepared using several methods, including fused deposition manufacturing (FDM), liquid-frozen deposition manufacturing (LFDM), stereolithography (SLA), digital light processing (DLP), selective laser sintering (SLS), power bed and inkjet head 3D printing (PIP), laminated object manufacturing (LOM), and digital beam melting (EBM) [12, 18]. SLA is often chosen as the fabrication method when customized materials with high precision are required [10]. SLA uses continuous layer-wise polymerization of UV-sensitive polymers to prepare the designed models through a curing process, namely photopolymerization [19]. However, there is a limited number of suitable resins that can be used in the SLA technique. Basically, the pre-resin should have low molar mass and preferably no crystallinity to ensure that its viscosity is low enough to be used in SLA [20]. Therefore, one of the most important limitations of SLA is the low variety of biopolymers used as a resin in this technique.

Until now, only few biopolymers, both synthetic and natural, have been reported and used for preparation of human scaffolds via the SLA technique, such as poly(D,L-lactic acid) (LA) [21], poly(ε-caprolactone) (PCL) [22], poly(trimethylenecarbonate) (PTMC) [23], poly(propylene fumarate) (PPF) [11, 24], polyethylene glycol diacrylate (PEGDA) [25], cellulose [26], and chitosan, gelatin and their copolymers [20, 27]. In addition, these biopolymers are well tolerated by cells in culture and tissues. However, they are often weak or lack the required elasticity; they do not have mechanical and/or physical properties comparable to natural tissues. These biopolymers are either stiff/brittle with low elongation, or are very soft with relatively low strength [28, 29]. Therefore, they cannot be used as heart or blood vessels, skeletal muscle, or tendon, because high elasticity and strength are needed for these applications. Polyurethanes (Pus) with a large diversity of chemical compositions have been extensively used in biomedical fields, especially in soft tissue regeneration, and they continue to gain interest due to their tunable mechanical properties and flexibility [30]. PUs are special groups of elastomeric block copolymers that are composed of "soft" rubbery segments and "hard" glassy or semicrystalline segments. A relatively long and flexible component, such as polyether or polyester diols, is used to contribute the soft segment, while a diisocyanate component and a low molecular weight diamine or diol as chain extender, are used to contribute hard segment [31, 32].

In the past years, research on biomedical engineering and tissue regeneration, biodegradability and biocompatibility of PUs has attracted considerable attention. Recently, Niu *et al.* demonstrated rat glial cell proliferation on PCL and PEG-based PUs for nerve tissue engineering with suitable mechanical and biodegradation properties [33]. Barrioni *et al.* attributed the moderate cytotoxicity of PCL and PEG-based PU encountering osteoblast cells after 24 h to the hard segment degradation

products [30]. Li *et al.* reported the electroactive PEG and PCL-containing PU films combining with aniline trimer (AT) for skin tissue application. They showed the proliferated L929 cells and promoted the wound healing process *in vivo* [34]. However, an investigation of the biodegradability, biocompatibility, and cell behaviour of 3D-printed PU-containing PCL and PEG segments, as well as a comparison with cast film systems, is still missing.

To this end, due to the high demand of PUs for tissue engineering [35, 36], we propose an elastic 3D-printed PU-scaffold for soft tissue regeneration, with high cell attachment and proliferation. Here, we studied the thermal and mechanical properties, degradation profile, toxicity, and the cell behaviour of PUs using different diols. To this end, three kinds of PUs were fabricated, using PCL and/or PEG diols as the soft segments through a solvent free method. Hydroxyethyl methacrylate (HEMA) was also used to functionalize the end of PUs to form photocurable-PU resins. The effects of different types of diols on the degradation, thermal and mechanical properties, hydrophilicity, biocompatibility, and their cell attachment of PUs were evaluated using several techniques. In addition, the role of scaffold geometry in fibroblast cell attachment was evaluated, and the results of cytotoxicity and cell behaviour of printed scaffolds were compared with cast film ones.

2. Experimental

2.1. Materials

Polycaprolactone diol (PCL, Mn 530 g mol^{-1}), polyethylene glycol (PEG, Mn 400 g mol^{-1}), hexamethylene diisocyanate (HDI, 98%), dibutyltin dilaurate (DBTDL, 95%), hydroxyethyl methacrylate (HEMA), propylene carbonate, 4-(2-hydroxyethyl)-1-piperazineethanesulfonic acid (HEPES), glutaraldehyde solution (25 wt % in H_2O), and dimethyl sulfoxide (DMSO) were purchased from Sigma-Aldrich. Ethyl

phenyl(2,4,6-trimethylbenzoyl)phosphinate was obtained from Carbosynth and Orasol Orange G was provided by BASF (Germany). Phosphate buffer solution (pH 7.4) was purchased from USP and FF-Chemicals, Finland. All chemicals were used as received. Fetal bovine serum (FBS), Dulbecco's Modified Eagle's Medium (DMEM), nonessential amino acids (NEAA) L-glutamine, and penicillin-streptomycin were obtained from HyClone, USA. Hank's Buffered Salt Solution (HBSS, 10×) and sodium pyruvate was obtained from Gibco Life Technologies. Dr. Christopher Jackson, Mitochondral Medicine University of Helsinki, Finland, kindly provided human dermal fibroblasts.

2.2. Synthesis of polyurethane resin

A series of PU resins were synthesized through a solvent-free, two-step polymerization process (Scheme 1), according to the following procedure. PCL and PEG were used as the macrodiol, either alone or in the mixture. For the preparation of the pre-polymer, a mixture of PCL diol and/or PEG diol, together with DBTDL (catalyst), were fed into a three-neck round-bottom flask reactor. Nitrogen flow was maintained for 20 min to provide an inert atmosphere. The mixture was stirred for 30 min at 60 $^{\circ}$C. Then, HDI was added dropwise to the mixture and the reaction proceeded for another 1 h at 60 $^{\circ}$C under N_2 atmosphere, yielding an isocyanate-ended, viscous pre-polymer. Afterwards, HEMA was added slowly to the pre-polymer and the reaction was stirred for a further 1 h at 60 $^{\circ}$C. Finally, the obtained viscose resin was diluted with propylene carbonate 40% w/w. The resin was stored in a cool and dark place to avoid crosslinking. The molar ratio of diol:HDI:HEMA was kept constant at 2:3:2 for all PUs, as summarized in Table 1. The prepared PUs were named according to the diol employed; for example, PU/PCL indicates that PCL was the diol,

PU/PEG indicates that PEG was the diol and PU/PCL/PEG indicates that both PCL and PEG were used as diol.

Table 1

The molar ratio of diol: HDI: HEMA for the synthesis of PU elastomers.

PU elastomers	PCL diol (mol)	PEG diol (mol)	HDI (mol)	HEMA (mol)
PU/PCL	0.02	-	0.03	0.02
PU/PEG	-	0.02	0.03	0.02
PU/PCL/PEG	0.01	0.01	0.03	0.02

2.3. 3D printing of resin using SLA

The SLA method was used for the 3D-printing of PU/PCL/PEG resin. To this aim, a certain amount of resin was transferred to a dark colored vial. Then, ethyl phenyl(2,4,6-trimethylbenzoyl)phosphinate (1.5 wt% relative to the resin) and Orasol Orange G as dye were added and mixed for 24 h to obtain a homogeneous mixture. For measuring the exact amount of dye, a calibration curve was prepared as described next. At first, a drop of resin without dye was illuminated for 10 s by a 50 mW laser power in the SLA device, and the thickness of cured resin was measured to obtain curing depth. Then, dye was added stepwise, with a content of 0.02, 0.04, and 0.06 wt% relative to the resin, and curing depths were determined. Finally, the exact amount of dye was measured (0.07 wt%) by extrapolating the curve to reach a thickness of 50 μm.

A commercial SLA device (Formlab 1+) was used to fabricate all 3D structures. A cylindrical porous 3D structure with a diamond pore architecture was prepared using

Mathmod 3.1 (https://sourceforge.net/projects/mathmod/) and the dimensions were modified and converted into printable files with the STL format using the Rhinoceros 3D CAD software (Robert McNeel and associates). The fabrication process was carried out by a 50 mW violet (405 nm) laser beam. The printing resolution was 250 μm in the xy direction and 5 μm per layers. In this study, the layer thickness was adjusted to 50 μm using Orasol Orange G as a neutral absorber in order to control the penetration depth of light into the resin. After printing, 3D objects were extracted with 1:1 propylene carbonate and ethanol mixtures for 24 h, pure ethanol for 24h, and finally dried at 40 °C for 24 h. No post curing was performed.

2.4. Characterization

Infrared (IR) spectroscopy was used to investigate the chemical structures of materials, using an attenuated total reflectance (ATR–IR) Perkin Elmer spectrometer in transmission mode. The scanning number and resolution were 16 and 4 cm^{-1}, respectively.

^{1}H-NMR and ^{13}C-NMR analyses were carried out with a Bruker AVANCE-III 400 MHz spectrometer, operating with sample solutions of $CDCl_3$ contains TMS as the internal standard and with 32 and 128 scans respectively, at room temperature. Chemical shifts were given in the δ scale in parts per million (ppm).

The polydispersity and molecular weight of the synthesized polymers were measured by Gel permeation chromatography (GPC), using the Water 717 Plus Autosampler device, equipped with two Agilent 5 μm mixed bed columns. Chloroform was used as a solvent, and applied at a flow rate of 1.0 mL min^{-1}. The sample concentration was ~ 1 mg mL^{-1}. Narrow molar mass distribution polystyrene standards were used for the calibration of the columns.

Tensile analysis was carried out using cast film PU (L = 20 mm, W = 5 mm, T = 0.2 mm) on Instron 4204 universal testing equipment. The static load cell was 100 N with a speed of 10 mm min^{-1}, and the measurement was done at 25 °C, with a relative humidity of 50%. All samples were stored at the testing conditions (25 °C, 50% relative humidity) for 48 h prior to testing.

The thermal stability of synthesized PU elastomers was measured by thermogravimetry analysis (TGA), operating a TA instrument (Q500) under N_2 atmosphere at a heating rate of 10 °C min^{-1} from 30 °C to 600 °C.

Differential scanning calorimetry (DSC) measurements were performed with a Q2000 device (TA Instruments) to analyze all three PUs. Samples were heated to 200 °C at a rate of 10 °C min^{-1}, followed by cooling to −70 °C. After equilibration at −70 °C for 5 min, a second heating cycle was performed to 200 °C at a rate of 10°C min^{-1}.

X-ray diffraction (XRD) was used to characterize the nature of the PUs. XRD patterns were collected using PANalytical X`Pert Powder XRD (alpha-1) diffractometer with a copper target at the wave length of λ CuKα = 1.5406°A, a tube voltage of 45 kV, and tube current of 40 mA, in the range of 5–100° at the speed of 0.05 ° min^{-1}.

Scanning electron microscopy (SEM) was used to examine the morphology of the 3D-printed scaffold and cell attachment on the surface of PUs, using Entry-level SEM (Zeiss sigma VP) with an accelerating voltage of 8 kV.

2.5. Rheology test

The rheology profile of PU/PCL/PEG resin was studied on a Physica MCR 301 Rheometer (Anton Paar) with measuring plate PP25/TG (25 mm) at 23 °C. After starting measurement for 50 s, the resin was irradiated with UV at an intensity of 50 MW cm^{-2} and the storage modulus changes were examined.

2.6. In vitro hydrolytic degradation

For *in vitro* degradation studies, 3D-printed scaffolds were submerged in 10 mL phosphate buffer solution (PBS, pH = 7.4), in sealed tubes and agitated with a shaker at a constant rate of 90 rpm at 37 °C for 6 months. The weight of samples was measured each month, and each measurement was averaged over 3 samples. For each measurement, the samples were removed from vials at the given time, wiped using tissue paper, dried under vacuum at 40 °C for 48 h, and then weighed. The PBS was renewed every month. The weight loss was calculated according to Eq. (1):

$$\text{Weight loss [\%]} = {}^{(W_0 - W_t)}/_{W_0} \times 100 \quad (1)$$

where, W_0 is the weight of sample before degradation and W_t is the weight of the sample at the given time.

2.7. Water absorption capacity

Water absorption capacity was investigated for all 3D-printed scaffolds according to Eq. (2). 3D-printed PUs were dried at 60 °C for 24 h, and then weighed (M_1). The samples were submerged in 10 mL distilled water separately and were kept in the shaker at a constant rate of 90 rpm at 37 °C for 1, 2, 3, and 4 days. The samples were weighed after removing excess water from the surface by wiping with tissue paper (M_2). The tests were performed in triplicate and averaged.

$$\text{Water absorption percent} = {}^{(M_2 - M_1)}/_{M_1} \times 100 \quad (2)$$

2.8. In vitro studies

2.8.1. Cell culture and culturing

Human dermal fibroblast cells were cultured in DMEM + 10% FBS, 1% NEAA, 1% L-glutamine, 1% penicillin-streptomycin, and 1% sodium pyruvate in 25 cm^2 cell culture flasks at 37 °C in 5% CO_2 until obtaining 80% of cell confluence before starting the tests.

2.8.2. Biocompatibility and cell attachment studies

The prepared resins were printed in 10 layers (~500 μm thick) and cut into circular samples by punching with a hollow tube with a diameter of 1 cm, and they were then sterilized in 70 vol% of ethanol, and washed twice with PBS buffer. For comparison, PU films with rough (spotted) and smooth surfaces were also fabricated through the traditional casting method.

The biocompatibility and cytotoxicity of cast film and printed PU films were investigated using two different assays: one of 3-(4,5-dimethylthiazol-2-yl)-2,5-diphenyltetrazolium bromide (MTT), and one of AlamarBlue. The cytotoxicity of the scaffolds was studied by the indirect method of replacing the medium containing degrading scaffold with the medium of the cell (extraction method), while the viability of the attached cells on the surface of the scaffold was studied by the direct method [37, 38], as explained in supporting information.

In addition, cast film and printed scaffolds were sterilized by UV and immersed inside DMEM + 10% of FBS for 24 h. About 20000 dermal fibroblast cells were counted and seeded on the rough (spotted) and smooth surface of cast film PU elastomers and 3D printed scaffolds to check the attachment and morphology of the cells. At each time point, the samples were washed by 1 × PBS (pH 7.4) and fixed by 2.5% of glutaraldehyde in 1 × PBS for 30 min at 37 °C. Samples were washed twice with 1× PBS (pH 7.4), and post-fixation was done by using 1% osmium tetroxide in

PBS for 1 h, followed by dehydration by ethanol (50, 70, 96, and 100%). Cell attachment was examined by SEM, and the samples were coated with gold.

2.9. Statistical analysis

Statistical analysis was done with one-way analysis of variance (ANOVA), with the level of significance set at $p < 0.01$ and $***p < 0.001$, using OriginPro8.6 software (OriginLab Corp.). The results are presented as means ± standard deviations (S.D.) of at least four independent sets of measurements.

3. Results and discussions

3.1 Resin synthesis

PU (PU/PCL/PEG) was fabricated using HDI as diisocyanate, and low molecular weight PCL and PEG microdiols as soft segments. HDI was used for the synthesis of PUs, because aliphatic isocyanate-based PUs have better light stability and lower toxicity compared to aromatic isocyanate-based ones [39, 40]. PCL and PEG were also introduced into the polymer backbone to improve the degradability and biocompatibility of PU, since the PCL and PEG segments can enhance the polymer's hydrolytic process and flexibility as a result of its components of hydrophilic PEG and flexible PCL [30, 41]. In addition, by using these two microdiols, good mechanical properties were expected to be achieved [42, 43]. For comparison, PU/PCL and PU/PEG resins were also synthesized to investigate the effect of diol variation on PU properties. Scheme 1 shows the synthesis of photocurable PU resins through a solvent-free method. During the first step, polymer chains were grown, and the viscosity increased over time. For controlling the viscosity, HDI was added dropwise to the mixture, and to ensure a PU with isocyanate end groups, the molar ratio of diol:HDI was kept at 2:3. As our main objective was to obtain photocurable PU resin in order to prepare 3D-printed PU through the SLA technique, in the second step, the NCO end

groups of pre-polymer were reacted with HEMA. In this way, the methacrylic groups were incorporated into the PU end chain, which are active sites for participating in the photo-crosslinking reaction and growing polymeric networks. Finally, high resolution 3D-printed PU with complex geometry was produced using the SLA technique, as discussed in next sections. For investigating the effect of the scaffold geometry *in vitro*, rough (spotted) and smooth PU films were also fabricated through the traditional casting method and tested with dermal fibroblast cells.

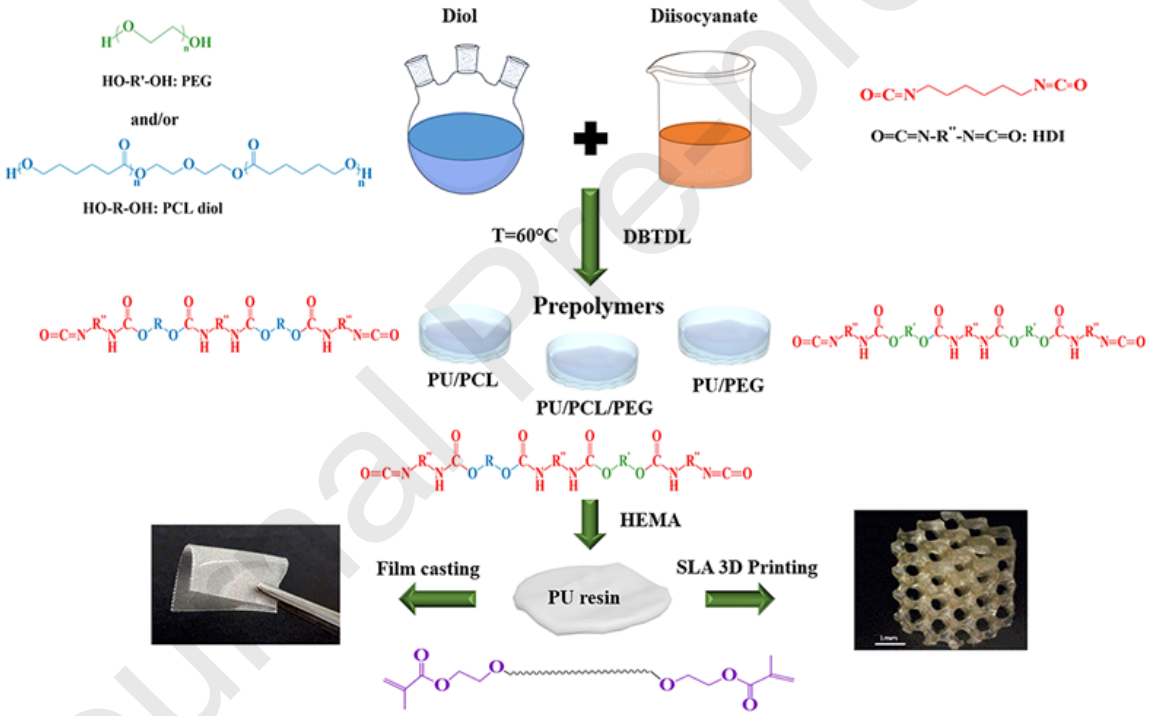

Scheme 1. A schematic of the preparation process of photocurable PU resins, 3D-printed PU scaffold and PU film.

3.2 Resin characterization

3. 2.1. NMR analysis

The molecular structure of the three PUs was confirmed using NMR. Fig. 1a displays the ^{1}H-NMR spectra of the PU/PCL/PEG pre-polymer and resin. The ^{1}H-

NMR spectra of PU/PCL and PU/PEG pre-polymer and resin are also presented in Fig. S1 and S2. Successful PU/PCL/PEG pre-polymer synthesis was confirmed with the characteristic ^{1}H peaks of the PCL, PEG and urethane groups (Fig. 1a). The peak at 3.67 ppm is assigned to the characteristic peak of PEG –(CH_2-CH_2-O)– groups and the peak at 4.05 ppm is attributed to the characteristic peak of PCL –CH_2-O– groups. Moreover, the characteristic peaks of –NH and –NH-CH_2– groups of urethane segments confirmed the successful preparation of the PU/PCL/PEG pre-polymer. After the reaction of isocyanate end groups of the pre-polymer with HEMA, the appearance of two characteristic peaks at 5.60 and 6.13 ppm, suggested that the PU/PCL/PEG pre-polymer was functionalized with methacrylate groups, which are essential parts for crosslinking and growing the network in 3D printing by SLA technique. In addition, the peaks at 1.96 and 4.31 ppm in the ^{1}HNMR spectrum of the PU/PCL/PEG resin were attributed to the –CH_3 and –CH_2-O– groups of HEMA, respectively. Moreover, the peak at 3.31 ppm in PU/PCL/PEG pre-polymer spectrum was attributed to O=C=N-CH_2– groups and was completely eliminated in the PU/PCL/PEG resin ^{1}H-NMR spectrum. All these observations confirmed the successful pre-polymer synthesis and functionalization with methacrylate groups using HEMA.

^{13}C-NMR was also employed for further confirmation of the synthesized PU re-polymers and resins. Fig. 1b presents the ^{13}C-NMR spectra of the PU/PCL/PEG pre-polymer and resin. The ^{13}C-NMR spectra of PU/PCL and PU/PEG pre-polymers, and resin are also presented in Fig. S3 and S4. In the ^{13}C-NMR spectrum of the PU/PCL/PEG pre-polymer, the characteristic peaks at 173.5, 156.5 and 70.6 ppm are assigned to PCL esteric carbonyl group, urethane C=O and –CH_2-O– groups of PEG segments, respectively, which confirmed the successful preparation of PU/PCL/PEG

pre-polymer. In the ^{13}C-NMR spectrum of the PU/PCL/PEG resin, new peaks appear at 167.1 (HEMA carbonyl group), 136.1 (methacrylate carbon double bond), 126.0 (methacrylate carbon double bond), 66.5 (HEMA methylene group), 61.1 (HEMA methylene group) and 18.4 (CH_3) ppm, suggesting the successful functionalization of PU/PCL/PEG pre-polymer with HEMA.

Fig. 1. (a) ^{1}H-NMR spectra of PU/PCL/PEG pre-polymer and resin in $CDCl_3$. (b) ^{13}C-NMR spectra of PU/PCL/PEG pre-polymer and resin in $CDCl_3$, R: PCL, R': PEG and R": HDI segments. (c) The ATR spectra of PU/PCL/PEG prepolymer, resin and elastomer. (d) XRD patterns of PU/PCL, PU/PEG and PU/PCL/PEG elastomers.

3.2.2. IR analysis

The chemical structures and formation of pre-polymer, PU resins and PU elastomers were further analyzed with ATR–FTIR. The spectra of the PU/PCL/PEG pre-polymer, resin and elastomer are presented in Fig. 1c. The IR spectra of the PU/PCL and PU/PEG prepolymer, resin and elastomer are also shown in Fig. S5 and

S6. In all PUs, the IR spectrum of pre-polymer shows characteristic bands at 3350 cm^{-1} (N-H stretching vibrations), 2850–3000 cm^{-1} (C-H stretching vibrations), 2250 cm^{-1} (N=C=O band), 1750 cm^{-1} (C=O band), and 1250 cm^{-1} (C-O band). The complete disappearance of the pre-polymer isocyanate peak and the appearance of a small band of C=C functional group at 1600–1680 cm^{-1}, confirmed that the pre-polymer was successfully reacted with HEMA, and the polymer chain was functionalized by methacrylate groups. The C=C band also disappeared during the light-initiated reaction of PU resin, which indicates that the acrylic C=C groups were involved in the crosslinking process of the polymer chains [44].

3.2.3 Gel permeation chromatography (GPC)

The weight average molecular weight (M_w), number average molecular weight (M_n), and polydispersity index (PDI) of all three PUs in $CHCl_3$ were calculated by GPC using polystyrene as a reference. The GPC results obtained are summarized in Table 2. The M_w of PUs ranged from 6.7 to 9.3 kDa, and the M_n of PUs ranged from 3.1 to 3.9 kDa. The resins used in the SLA technique were expected to have low viscosity and molecular weight, which is important in order to be able to flow and spread appropriately during the printing. This is important for certifying the accurate printing of each layer and getting into solidified rigid or flexible geometries [45, 46]. Therefore, the low values of M_n provided the low viscosity of the PU resins, which is expected to be suitable for 3D printing by the SLA method. Moreover, the relatively narrow PDI values showed that the prepared PU resins were relatively homogeneous.

Table 2

Gel permeation chromatography (GPC) results of prepared PUs in $CHCl_3$ and polystyrene as reference.

Sample	M_w (kDa)	M_n (kDa)	PDI

PU/PCL	9.3	3.9	2.4
PU/PEG	6.7	3.1	2.3
PU/PCL/PEG	9.1	3.6	2.5

3.2.4 XRD technique

Fig. 1d displays the XRD patterns of PU films. One sharp and broad peak is seen at 2θ = 21 °, and one broader peak with lower intensity is seen at 2θ = 45 ° in the diffractograms of PU-based films, which shows the amorphous nature of these polymers. Generally, low molecular weight PCL (<2000 g mol^{-1}) is amorphous, and its crystallinity can be reduced due to the existence of low molecular weight PEG segments in the polymer structure [47, 48]. Therefore, the amorphous property of the prepared PUs is due to the presence of PCL and/or PEG in the polymer backbone. The amorphous structure of PUs has significant advantages compared to semi-crystalline ones in terms of degradation, which is crucially important for tissue engineering applications [42].

3.3. PU elastomer properties

3.3.1. Thermal properties

The thermal properties of the synthesized PUs were studied, using TGA and DSC techniques, and the results are shown in Fig. 2. According to the TGA thermograms (Fig. 2a), the degradation onset temperature at 5 wt% loss ($T_{5\%}$) of PU/PCL, PU/PEG, and PU/PCL/PEG were 258, 291, and 305 °C, respectively. Moreover, the thermal degradation of all prepared PUs proceeded in two major steps, and about 80% of them by weight was lost in the 250–380 °C temperature range. The first weight-loss step (T_{max1}) can be due to the decomposition of urethane, ether, and/or ester groups [49, 50]. The decomposition of urethane bonds leads to the formation of alcohols and

isocyanates, while the decomposition of ester and ether bonds in PCL and PEG, respectively, is attributed to chain scission [51]. The second weight loss (T_{max2}), which occurred between 420–460 °C was assigned to the cleavage of C–C bonds [50]. The T_{max1} and T_{max2} for PU/PCL were 366 °C and 443 °C, with content degradations of 85% and 13%, respectively. For PU/PEG, T_{max1} and T_{max2} were 358 °C and 447 °C, with content degradations of 77% and 20%, respectively. For PU/PCL/PEG, these temperatures were 373 °C and 448 °C, with content degradations of 74% and 24%, respectively. The results showed that PU/PCL/PEG and PU/PCL were more thermally stable than PU/PEG, which may be due to the higher thermal stability of esteric bonds compared with ether bonds [52]. In general, all these three PUs are thermally stable over 250 °C, which could be beneficial for high temperature sterilization of the scaffold before clinical using [53].

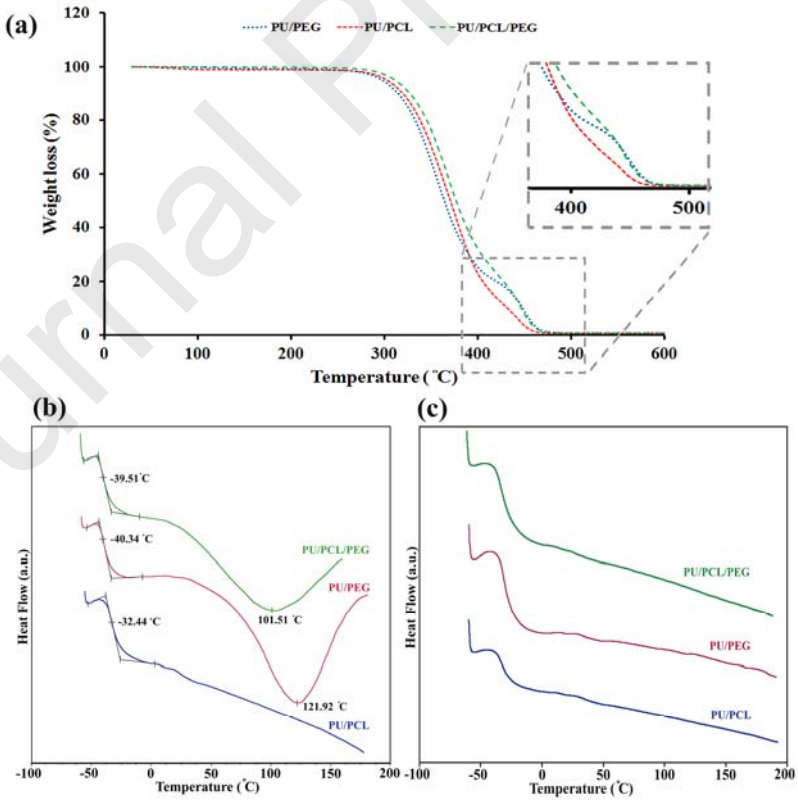

Fig. 2. (a) TGA curves of PU/PCL, PU/PEG and PU/PCL/PEG resins with the heating rate of 10 °C min^{-1}. (b) and (c) The DSC first and second heating scans of PU/PCL, PU/PEG and PU/PCL/PEG resins.

DSC analysis was used to determine PU crystalline and glass transition properties. The first and second heating scans of PU/PCL, PU/PEG, and PU/PCL/PEG resins are presented in Fig. 2b and 2c. The corresponding transition data, including the glass transition temperature (T_g) and melting temperature (T_m) are also shown in Fig. 2b. The first heating scan of PU/PEG and PU/PCL/PEG (Fig. 2b) showed melting peaks at 121.92 and 101.51 °C, respectively, which are related to the melting of the remaining crystalline regions rich in PEG. No melting peak was found for the PU/PCL resin due to the amorphous nature of low molecular weight PCL, as discussed in the XRD section above. PU/PCL/PEG showed a wider melting peak compared to PU/PEG, which may be due to the incorporation of the PCL segment in the polymer structure, reducing the crystallizing ability of the polymer. In the second heating scan (Fig. 2c), for both PEG-containing resins, no T_m was observed, which confirmed the amorphous nature of PUs. According to the DSC thermograms, PU/PCL, PU/PEG, and PU/PCL/PEG resins showed T_g at –32.44, –40.34, and –39.51 °C, respectively, which means that they are in a rubbery state at room temperature [54, 55]. In addition, for all three resins, only one T_g was observed, indicating that there was no phase separation in the polymer structure. Generally, in a segmented PU structure, two separate T_m and two distinct T_g values are frequently observed for the soft and hard segments if the hard and soft phases were completely immiscible. According to our DSC results, the hard and soft segments are completely miscible.

3.3.2. Mechanical properties

Mechanical performance is one of the most important features needed for tissue engineering scaffolds. The mechanical properties of PU elastomers were characterized using a film tensile test with a pulling rate of 10 mm min^{-1}. Representative stress-strain curves of PU/PCL, PU/PEG, and PU/PCL/PEG elastomers are shown in Fig. 3a. The mean values for five specimens of each were measured, and the calculated mechanical parameters are summarized in Table 3. The difference in diols in the PU samples causes their measured mechanical properties to differentiate. Among these samples, the PU/PCL/PEG elastomer showed the highest tensile stress (3.33 MPa) and tensile strain (145%), with a Young's modulus of 4.48 MPa. The results demonstrate that the PU/PCL/PEG elastomer is more flexible and has a much higher tensile strength compared to the others, and its mechanical properties are in the range of values needed for soft tissue engineering applications [56, 57] and are close to the mechanical properties of native soft tissues, especially skin tissues [10, 58, 59].

In addition, the PU elastomers synthesized here were investigated for elastic recovery behavior, using a static creep test at an applied stress of 1 MPa at room temperature (Fig. 3b). The samples showed very fast recovery immediately after releasing the force and almost recovered to 95% of its original length. These results showed that, on the molecular level of the PU elastomer, there are flexible segments cross-linked together with chemical bonds. These properties are associated with the good flexibility of the PU elastomers, and they are key features for tissue engineering applications. Since most human tissues, including skin, heart, liver, muscle, and blood vessels prefer elastic implants with good mechanical strength that can maintain their properties over the time [10]; PU/PCL/PEG can be a good candidate for soft tissue engineering.

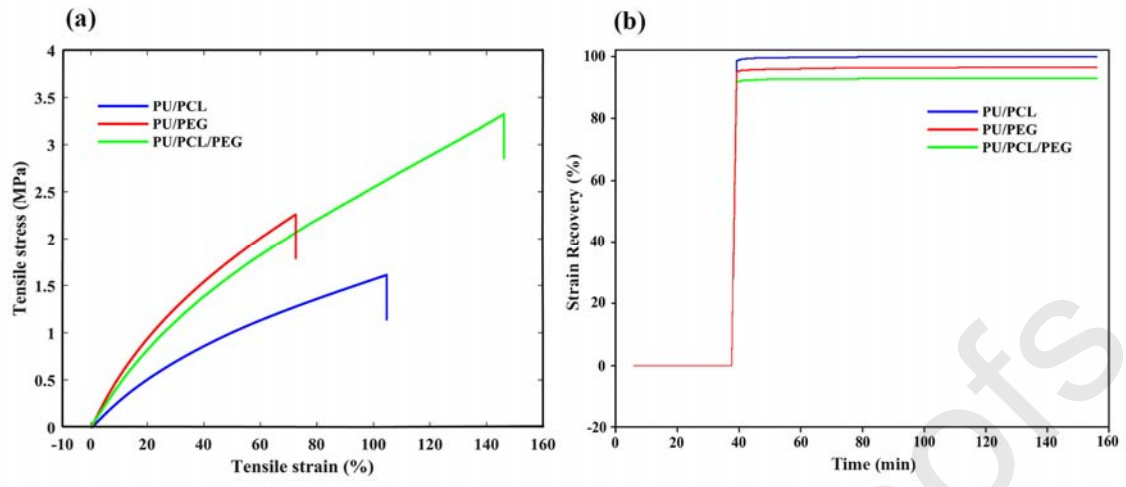

Fig. 3. (a) Stress-strain curves of PU/PCL, PU/PEG and PU/PCL/PEG elastomers. (b) Elastic recovery property of PU/PCL, PU/PEG and PU/PCL/PEG elastomers at an applied stress of 1 MPa.

Table 3

Mechanical properties of synthesized PUs (n = 5, average ± SD).

Sample	Young's Modulus (MPa)	Tensile stress (MPa)	Tensile strain (%)
PU/PCL	2.88 ± 0.08	1.64 ± 0.15	105.00 ± 8.98
PU/PEG	5.57 ± 0.27	2.26 ± 0.12	72.00 ± 8.95
PU/PCL/PEG	4.48 ± 0.10	3.33 ± 0.25	145.00 ± 7.60

3.3.3 Rheological analysis

As a result of the higher tensile stress and strain of PU/PCL/PEG, and its favorable Young's modulus, it was selected as the best resin for the preparation of 3D printed scaffold suitable for tissue engineering. On this basis, the rheological changes of PU/PCL/PEG resin under

UV-irradiation were studied. Fig. 4 shows the evolution of the storage modulus (G') and loss modulus (G") of the PU/PCL/PEG resin before and during UV exposure at 50 mW cm^{-2}. Before UV exposure, G" is greater than G', indicating the predominantly liquid nature of the medium. Then, under UV irradiation, a very rapid reaction rate was seen, and the dynamic moduli G' and G" exhibited a crossover in about 3 sec. The sharp increase in G' and G" showed the formation of polymer gel with a curing time of 3 sec, which is very useful for layer-by-layer 3D printing in the SLA technique [45]. After the gel point (G' = G"), G' was greater than G", and constant values were observed, revealing the predominantly viscoelastic solid behavior of PU/PCL/PEG and completion of crosslinking process [60].

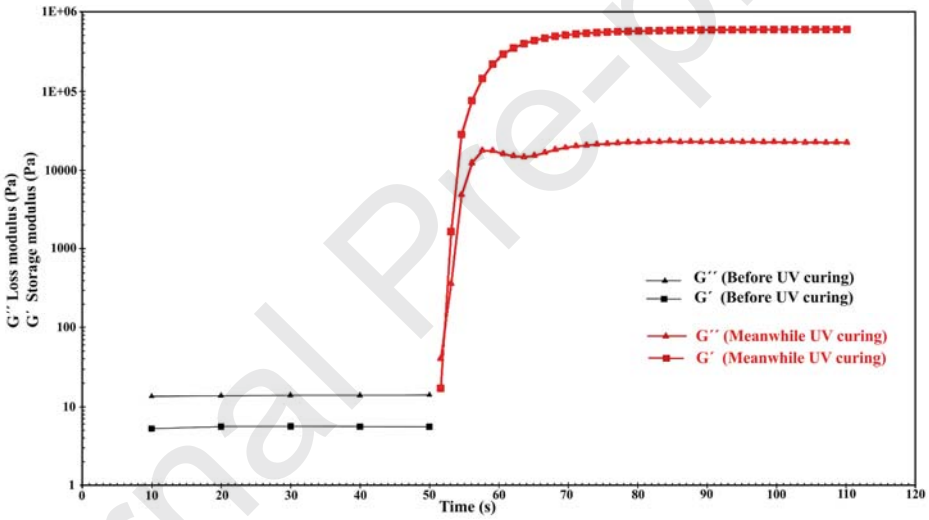

Fig. 4. Dynamic Moduli (G' and G") plotted as a function of time for a 50 mW UV exposure.

3.4. 3D printing with SLA

The SLA set-up for the fabrication of 3D printed scaffolds is presented in Fig. 5a. The prepared UV-sensitive and low molecular weight PU resin was poured into a transparent tank, and the build platform was moved up out of the resin while continuous layer-by-layer photopolymerization was performed. In this way, each newly formed layer crosslinked into the previous layer until a 3D crosslinked structure was built on the moving platform. In this step, the curing depth is important; it should

be deep enough to make the layers attach to each other and form an adequately porous structure. The cure depth of the resin was controlled by the addition of Orasol Orange G dye in the resin. Finally, after the extraction of the dye by immersing the 3D-printed scaffold in propylene carbonate/ethanol solution, a highly transparent and porous 3D-printed PU scaffold was obtained. The homogeneous porous structure of the 3D-printed PU/PCL/PEG scaffold was then observed under SEM (Fig. 5b). The layered structure of the scaffold, with high porosity, together with interconnected/lined pores, can also be clearly observed in the SEM images.

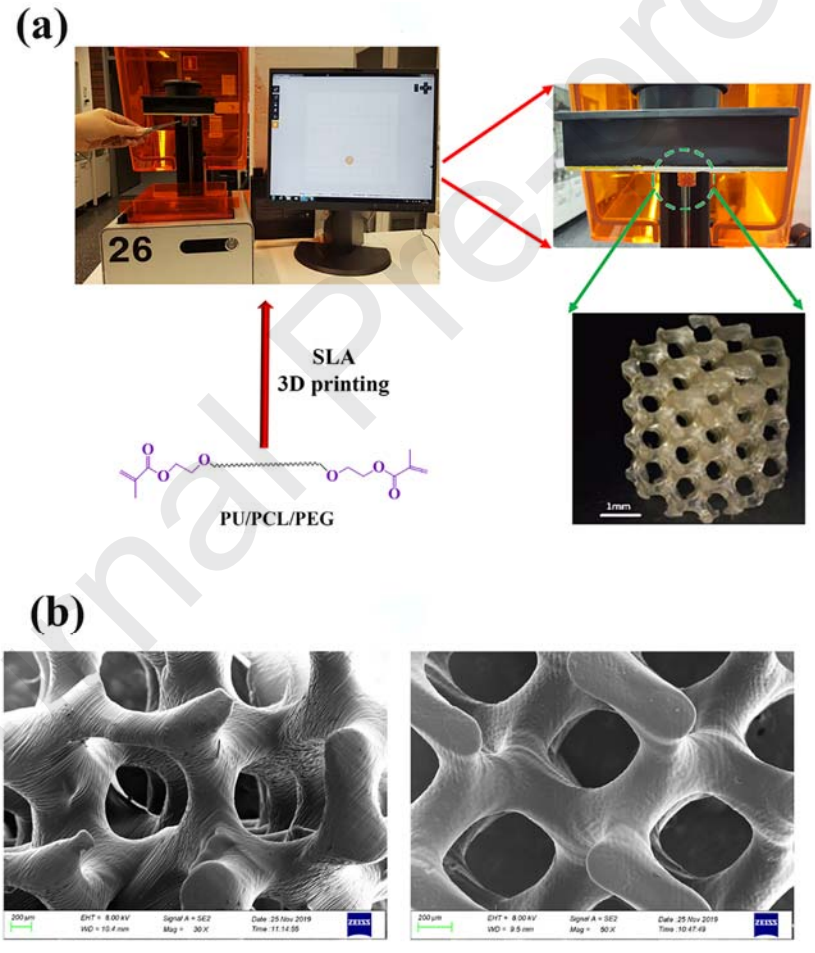

Fig. 5. (a) Manufacturing set up for 3D printed scaffold from photocurable PU/PCL/PEG resin using SLA technique. (b) SEM images of 3D-printed PU/PCL/PEG scaffold at magnification of 200 μm.

3.5. Water absorption capacity

Since the hydrolytic degradation of scaffolds is one key factor in tissue engineering, it is important to examine the water absorption capacity of 3D-printed PU scaffolds and characterize their hydrophilicity. The water absorption (%) of the 3D-printed PU/PCL, PU/PEG, and PU/PCL/PEG scaffolds immersed in deionized water was investigated for 4 days, and the results are presented in Fig. 6a. PU/PEG absorbed water more than the others (overall ~40%), which is due to the hydrophilic nature of PEG. PU/PCL/PEG showed higher water absorption capacity than PU/PCL, demonstrating the influence of PEG on water absorption capacity. In tissue engineering, hydrophilicity is important because scaffold wettability affects cell spreading and adhesion [14, 61].

3.6. In vitro hydrolytic degradation

In addition to suitable mechanical and thermal properties, hydrolytic degradation is another important feature required for long-term scaffolds used in tissue engineering. The weight loss method was applied in order to investigate the *in vitro* hydrolytic degradation of the prepared PUs in PBS (PH = 7.4) at 37 $^{\circ}$C. Fig. 6b shows the time dependence of the weight loss for different PUs. The range of degradation values for the PU/PCL sample is from 1% (month 1) to 6% (month 6). The PU/PEG sample exhibited the fastest degradation rate overall, ranging from 5% (month 1) to 30% (month 6). In general, ester and urethane bonds undergo hydrolysis, and the esters are expected to be more unstable than the urethanes [62]. PU/PEG contains only urethane bonds and was expected to be hydrolyzed into shorter PU chains. The most important

reason for the higher degradation property of PU/PEG is attributed to its gradual solubilization. The hydrophilic nature of PEG leads to an increased penetration of PBS into the scaffold, resulting in the enhancement of hydrolytic degradation over time. As shown in Fig. 6b, the PU containing only PCL degrades slowly, which may be due to the high hydrophobicity of PCL resulting in resistance to hydrolysis. As reported in the literature, the hydrolysis rate of the ester bonds in PCL-containing polymers is very low, especially at pH values around 7 [63]. Higher hydrolysis rates can be obtained in acidic or basic conditions or in the presence of enzymes [64, 65]. In the case of PU/PCL/PEG, the degradation values varied from 5% (month 1) to 18% (month 6), which was higher than the amount of PU/PCL degradation. Therefore, PEG-containing PUs are the best choice for tissue engineering applications, owing to their higher hydrophilicity and degradation rates.

To verify the ability of PBS to mediate the 3D structure of PU/PCL/PEG, changes in the volume of the scaffold before and after immersing in PBS solution were examined (Fig. 6c). After immersing in PBS, scaffold volume changes were clearly observed. Due to the hydrophilic nature of PEG segments, and also the amorphous nature of PU/PCL/PEG, as evidenced by XRD, PBS leads to an increase of the scaffold volume until degradation takes place.

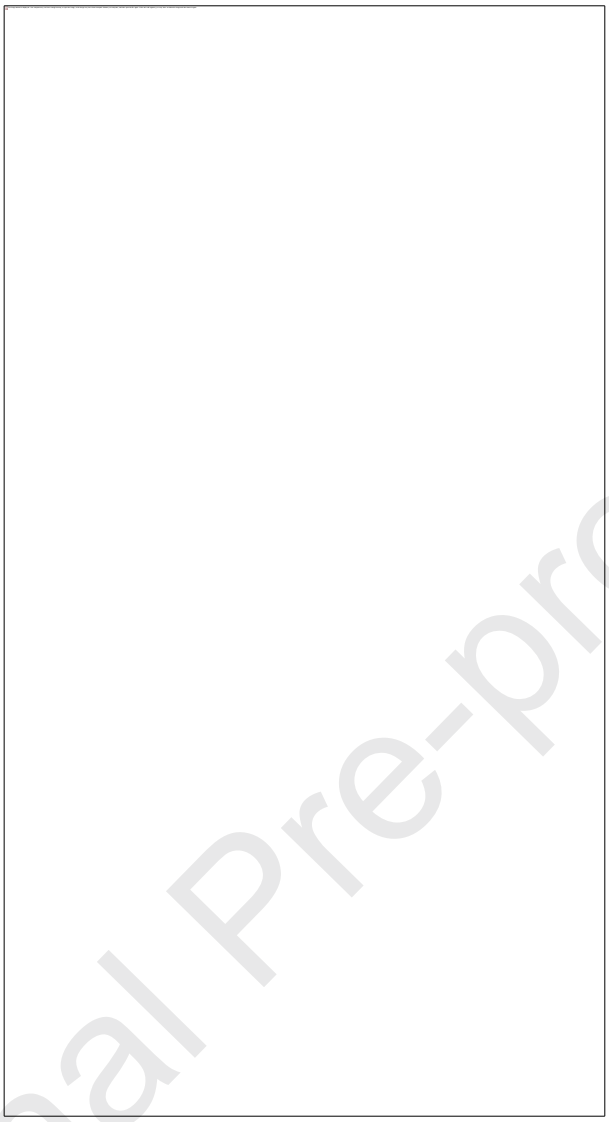

Fig. 6. (a) Water absorption capacity of the 3D-printed PU/PCL, PU/PEG and PU/PCL/PEG scaffolds immersed in deionized water for different periods of time. The results represent the average of three measurements. (b) Time dependence of *in vitro* hydrolytic degradation of PU/PCL, PU/PEG and PU/PCL/PEG in PBS at 37 °C. Data represent mean ± SD (n=3). (c) Camera picture of 3D-printed PU/PCL/PEG scaffold before and after immersing in PBS solution.

3.7. In vitro studies

The effect of the biodegradation products of printed scaffolds on fibroblast cells was investigated by extracting the medium containing degrading samples from the cell wells (extraction method) [38], using an MTT assay within 21 days (Fig. 7a). All three types of printed PU elastomers (PU/PCL, PU/PEG, and PU/PCL/PEG) showed high biocompatibility for three weeks with no sign of toxicity. Based on hydrolytic degradation results (Fig. 6b), around 5% degradation was seen in the first month due to slow bulk erosion, which provided a safe environment for cells, not only staying viable, but also showing proliferation. PU/PCL/PEG showed higher proliferation compared to PU/PCL and remained in the same range as PU/PEG. Therefore, based on the MTT results, PU/PEG and PU/PCL/PEG containing PEG-400 appear to be biocompatible, and the degradation mechanism and products of all three PU candidates are nontoxic to dermal fibroblast cells.

In addition, an AlamarBlue assay was used to assess the viability of the attached cells on the surface of 3D-printed PU scaffolds containing different diols. For comparison, these experiments were also performed on the rough and smooth surface of cast film elastomers to demonstrate the impact of the printed structures on cell viability and attachment (Fig. 7b). As can be seen, the cells on rough cast film PU/PCL, PU/PEG, and PU/PCL/PEG all showed cell viabilities of less than 60%. These results were almost the same for smooth cast film PU/PCL and PU-/PCL/PEG, except for PU/PEG. In the case of the smooth PU/PEG elastomer, the viability was on the lowest range of close to zero, which may be as a result of the low degree of attachment of the cells to the surface (this can also be seen in SEM images, Fig. S7). This may be due to the high hydrophilicity of PEG, as described in the degradation section above. It has previously been reported that PEG-based materials have cell-repulsive properties due to the hydrophilic nature of PEG [66]. Zhang *et al.* used PEG film to reduce the protein and cell attachment on silicon surfaces to prevent the fibrotic response of the system [67]. As shown

in Fig. 7b, in general, printed scaffolds showed better cell viability compared to cast film PUs and printed PU/PCL/PEG showed higher cell viability (~ 100%) compared to other printed PUs.

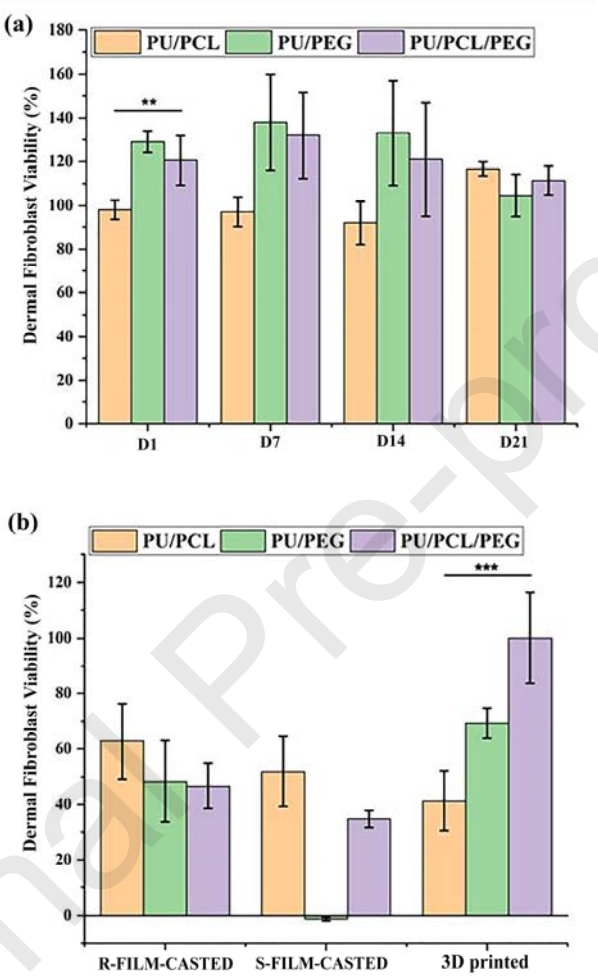

Fig. 7. (a) Cell viability of dermal fibroblast cells using MTT assay for PU/PCL, PU/PEG, and PU/PCL/PEG after 1, 7, 14 and 21 days of incubation (Extract method). (b) Cell viability of dermal fibroblast cells using AlamarBlue assay for rough (R) and smooth (S) cast films, 3D-printed PU/PCL, PU/PEG, and PU/PCL/PEG scaffolds (Direct method). Statistical analysis was done using a one-way analysis of variance (ANOVA) with the level of significance set at probabilities of $^{**}p < 0.01$ and $^{***}p < 0.001$.

According to the SEM images, fibroblast cells showed high elongation and infiltration with high proliferation on all three types of printed PU elastomers after 14 days (Fig. 8). As clearly seen in Fig. 8a, a high cell population on printed PU/PCL/PEG scaffold was observed at day 4. PU/PEG showed low cell attachment on day 4 compared to PU/PCL and PU/PCL/PEG, and the cell population increased at day 14 (Fig. 8c). As described before, this low cell attachment of PU/PEG may also be due to the hydrophilic and cell-repulsive nature of PEG. Consequently, printed PU/PCL/PEG scaffold showed the highest cell viability and proliferation when compared to PU/PCL and PU/PEG, which demonstrates the positive effect of the combination of PCL and PEG microdiols for biomedical applications, especially for skin regeneration.

For comparison, dermal fibroblast cell attachment on the surface of rough (R) and smooth (S) PU films at day 4 was also investigated, and the SEM images are shown in Fig. S7. While the cells could be trapped on 3D printed samples, they were not able to attach onto smooth surfaces with no roughness, especially on cast film PU/PEG. These results show the importance of PU geometry and texture made by the SLA method in attaching cells and providing a safe environment for them to remain viable for at least 3 weeks.

Based on the results, two factors could play a role both in attracting cells to the surface of the scaffolds and in their viability. While the morphology of the surface (rough and patterned made by 3D printing technique) could provide a suitable place for cells to attach, the physiochemical properties of the surface may play a significant role as well. In the case of PU/PEG scaffolds, although the hydrophilic PEG reduces the cell attachment, the texture and geometry of the surface were able to overcome the physiochemical properties, and cells could still attach to patterned 3D printed scaffolds with around 70% of viability. For PU/PCL

samples, the PCL surface properties could control the viability to a greater degree than geometry, and cells could show the same range of viability in all three types of scaffold surfaces. However, on smooth cast film PU/PCL, cell morphology was found to have changed, which may be due to the lack of a suitable attachment site on the surface. In the case of PU/PCL/PEG, both factors could determine both cell viability and attachment. While in smooth cast film samples, cell attachment and viability decreased, the rough surface texture was able to improve the cell attachment and viability to levels similar to the PU/PEG samples. 3D-printed PU/PCL/PEG showed the favorable properties of both polymers, while having the advantage of a patterned geometry conducive to cell attachment. Therefore, due to the high compatibility and cell attachment on the printed PU/PCL/PEG scaffold, it could be a good candidate for soft tissue engineering.

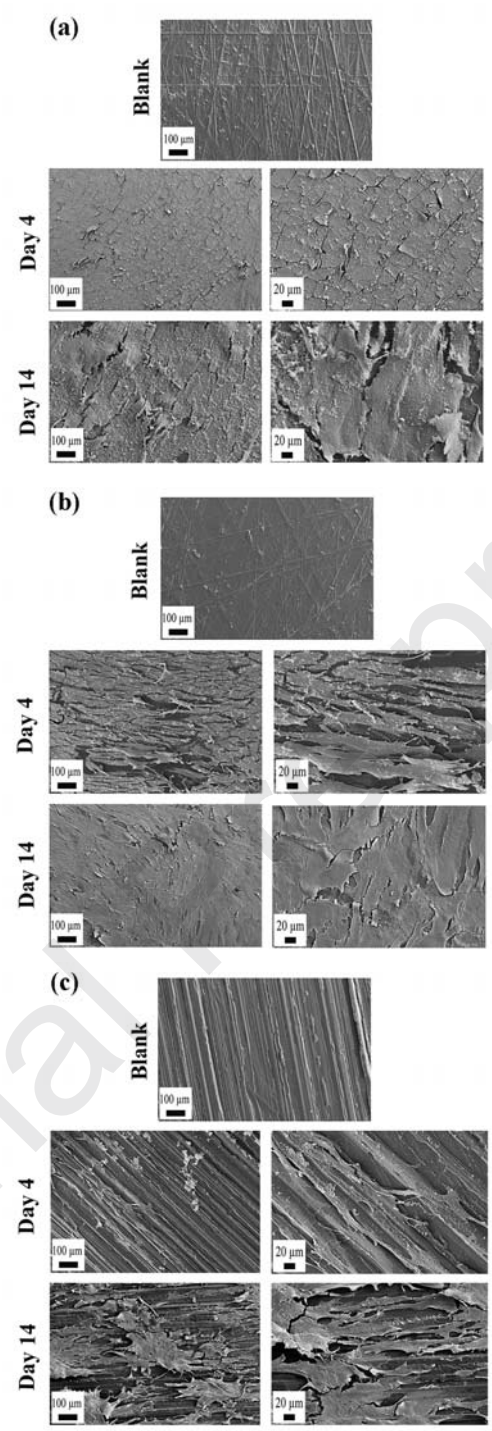

Fig. 8. (a) SEM images of printed PU/PCL/PEG (blank) and dermal fibroblast cell attachment on printed PU/PCL/PEG surface on days 4 and 14 at different magnifications. (b) SEM images of printed PU/PCL (blank) and dermal fibroblast cell attachment on printed

PU/PCL surface at days 4 and 14 at different magnifications. (c) SEM images of printed PU/PEG (blank) and dermal fibroblast cell attachment on printed PU/PEG surface at days 4 and 14 at different magnifications.

4. Conclusions

A biocompatible, degradable and elastic 3D-printed PU scaffold with a complex geometry and high resolution was fabricated using the SLA technique for soft tissue regeneration with high cell attachment and proliferation. PU/PCL/PEG exhibited a tensile stress of 3.33 MPa, tensile strain at break of 145%, and a Young's Modulus of 4.48 MPa with *in vitro* hydrolytic degradation of 18% after 6 months. Rheological characterization of PU/PCL/PEG under UV-irradiation revealed the formation of polymer gel with the curing time of 3 sec. The cell viability of dermal fibroblast cells by MTT and AlamarBlue assays confirmed that the printed PU/PCL/PEG scaffold had higher cell viability and proliferation compared to others, and revealed that PU/PCL/PEG degradation did not show any cytotoxicity effect under the conditions tested. In contrast to the low cell attachment of cast film elastomers, printed PU/PCL/PEG showed the best cell attachment and proliferation. Overall, these results demonstrate that 3D-printed PU/PCL/PEG scaffolds made by the SLA method have the potential to be applied in soft tissue engineering.

Supporting Information

^{1}H-NMR spectra of PU/PCL pre-polymer and resin in $CDCl_3$ (Fig. S1); ^{13}C-NMR spectra of PU/PCL pre-polymer and resin in $CDCl_3$ (Fig. S2); ^{1}H-NMR spectra of PU/PEG pre-polymer and resin in $CDCl_3$ (Fig. S3); ^{13}C-NMR spectra of PU/PEG pre-polymer and resin in $CDCl_3$ (Fig. S4); The ATR-IR spectra of PU/PCL prepolymer, resin and elastomer (Fig. S5); The ATR-IR spectra of PU/PEG prepolymer, resin and elastomer (Fig. S6); SEM images of

dermal fibroblast cell attachment on rough (spotted) and smooth cast film PU/PCL, PU/PEG and PU/PCL/PEG surface on day 4 at magnification of 100 μm (Fig. S7).

Notes

The authors declare no competing financial interest.

Acknowledgement

The authors would like to thank Magnus Ehrnrooth Foundation, Finnish Cultural Foundation, HiLIFE Research Funds, Sigrid Jusélius Foundation, and Academy of Finland (3D-Biomat project) for providing funding for this project. This work made use of BIOECONOMY infrastructure at Aalto University. The authors also acknowledge the Electron Microscopy Unit of the Institute of Biotechnology, University of Helsinki, for laboratory facilities and assistance.

References

[1] G. Ratheesh, J.R. Venugopal, A. Chinappan, H. Ezhilarasu, A. Sadiq, S. Ramakrishna, 3D Fabrication of Polymeric Scaffolds for Regenerative Therapy, ACS Biomater-Sci Eng 3(7) (2017) 1175-1194.

[2] M.S. Shoichet, Polymer Scaffolds for Biomaterials Applications, Macromolecules 43(2) (2010) 581-591.

[3] N. Iqbal, A.S. Khan, A. Asif, M. Yar, J.W. Haycock, I.U. Rehman, Recent concepts in biodegradable polymers for tissue engineering paradigms: a critical review, Int. Mater. Rev. 64(2) (2019) 91-126.

[4] J. Velema, D. Kaplan, Biopolymer-Based Biomaterials as Scaffolds for Tissue Engineering, in: K. Lee, D. Kaplan (Eds.), Tissue Engineering I, Springer Berlin Heidelberg, Berlin, Heidelberg, 2006, pp. 187-238.

[5] A. Kashirina, Y. Yao, Y. Liu, J. Leng, Biopolymers as bone substitutes: a review, Biomater Sci 7(10) (2019) 3961-3983.

[6] F. Asghari, M. Samiei, K. Adibkia, A. Akbarzadeh, S. Davaran, Biodegradable and biocompatible polymers for tissue engineering application: a review, Artif Cells Nanomed Biotechnol 45(2) (2017) 185-192.

[7] Q. Wang, X. Pan, C. Lin, D. Lin, Y. Ni, L. Chen, L. Huang, S. Cao, X. Ma, Biocompatible, self-wrinkled, antifreezing and stretchable hydrogel-based wearable sensor with PEDOT:sulfonated lignin as conductive materials, Chem. Eng. J. 370 (2019) 1039-1047.

[8] B. Dhandayuthapani, Y. Yoshida, T. Maekawa, D.S. Kumar, Polymeric Scaffolds in Tissue Engineering Application: A Review, Int. J. Polym. Sci 2011 (2011) 1-19.

[9] G.C. de Ruiter, M.J. Malessy, M.J. Yaszemski, A.J. Windebank, R.J. Spinner, Designing ideal conduits for peripheral nerve repair, Neurosurg. Focus 26(2) (2009) E5.

[10] R.J. Mondschein, A. Kanitkar, C.B. Williams, S.S. Verbridge, T.E. Long, Polymer structure-property requirements for stereolithographic 3D printing of soft tissue engineering scaffolds, Biomaterials 140 (2017) 170-188.

[11] Y. Luo, G. Le Fer, D. Dean, M.L. Becker, 3D Printing of Poly(propylene fumarate) Oligomers: Evaluation of Resin Viscosity, Printing Characteristics and Mechanical Properties, Biomacromolecules 20(4) (2019) 1699-1708.

[12] K. Tappa, U. Jammalamadaka, Novel biomaterials used in medical 3D printing techniques, J. Func. Biomater 9(1) (2018) 17.

[13] S. Bose, D. Ke, H. Sahasrabudhe, A. Bandyopadhyay, Additive manufacturing of biomaterials, Prog. Mater Sci. 93 (2018) 45-111.

[14] S. Pina, V.P. Ribeiro, C.F. Marques, F.R. Maia, T.H. Silva, R.L. Reis, J.M. Oliveira, Scaffolding Strategies for Tissue Engineering and Regenerative Medicine Applications, Materials 12(11) (2019) 1824.

[15] T. Fuoco, A. Ahlinder, S. Jain, K. Mustafa, A. Finne-Wistrand, Poly(-caprolactone-co-p-dioxanone): a Degradable and Printable Copolymer for Pliable 3D Scaffolds Fabrication toward Adipose Tissue Regeneration, Biomacromolecules 21(1) 2020 188–198 .

[16] A.M. Pekkanen, R.J. Mondschein, C.B. Williams, T.E. Long, 3D Printing Polymers with Supramolecular Functionality for Biological Applications, Biomacromolecules 18(9) (2017) 2669-2687.

[17] I. Matai, G. Kaur, A. Seyedsalehi, A. McClinton, C.T. Laurencin, Progress in 3D bioprinting technology for tissue/organ regenerative engineering, Biomaterials 226 (2020) 119536.

[18] S.C. Ligon, R. Liska, J.r. Stampfl, M. Gurr, R. Mülhaupt, Polymers for 3D printing and customized additive manufacturing, Chem. Rev. 117(15) (2017) 10212-10290.

[19] A. Goyanes, U. Det-Amornrat, J. Wang, A.W. Basit, S. Gaisford, 3D scanning and 3D printing as innovative technologies for fabricating personalized topical drug delivery systems, J. Controlled Release 234 (2016) 41-48.

[20] G. Taormina, C. Sciancalepore, M. Messori, F. Bondioli, 3D printing processes for photocurable polymeric materials: technologies, materials, and future trends, J Appl Biomater Func 16(3) (2018) 151-160.

[21] F.P. Melchels, J. Feijen, D.W. Grijpma, A poly(D,L-lactide) resin for the preparation of tissue engineering scaffolds by stereolithography, Biomaterials 30(23-24) (2009) 3801-9.

[22] S. Asikainen, B. van Bochove, J.V. Seppala, Drug-releasing Biopolymeric Structures Manufactured via Stereolithography, Biomed. Phys. Eng Express 5 (2019) 025008.

[23] K.E. Dienel, B. van Bochove, J.V. Seppälä, Additive Manufacturing of Bioactive Poly (trimethylene carbonate)/ -tricalcium phosphate Composites for Bone Regeneration, Biomacromolecules 21(2) (2020) 366–375 .

[24] K.W. Lee, S. Wang, B.C. Fox, E.L. Ritman, M.J. Yaszemski, L. Lu, Poly(propylene fumarate) bone tissue engineering scaffold fabrication using stereolithography: effects of resin formulations and laser parameters, Biomacromolecules 8(4) (2007) 1077-84.

[25] D.G. Tamay, T.D. Usal, A.S. Alagoz, D. Yucel, N. Hasirci, V. Hasirci, 3D and 4D printing of polymers for tissue engineering applications, Front Bioeng Biotech 7 (2019) 1-22.

[26] N.B. Palaganas, J.D. Mangadlao, A.C.C. de Leon, J.O. Palaganas, K.D. Pangilinan, Y.J. Lee, R.C. Advincula, 3D Printing of Photocurable Cellulose Nanocrystal Composite for Fabrication of Complex Architectures via Stereolithography, ACS Appl. Mater. Interfaces 9(39) (2017) 34314-34324.

[27] T. Matsuda, M. Mizutani, S.C. Arnold, Molecular design of photocurable liquid biodegradable copolymers. 1. Synthesis and photocuring characteristics, Macromolecules 33(3) (2000) 795-800.

[28] T.A. Folliguet, C. Rücker-Martin, C. Pavoine, E. Deroubaix, M. Henaff, J.-J. Mercadier, S.N. Hatem, Adult cardiac myocytes survive and remain excitable during long-term culture on synthetic supports, J Thorac Cardiovasc Surg 121(3) (2001) 510-519.

[29] M.C. Serrano, E.J. Chung, G.A. Ameer, Advances and applications of biodegradable elastomers in regenerative medicine, Adv. Funct. Mater. 20(2) (2010) 192-208.

[30] B.R. Barrioni, S.M. de Carvalho, R.L. Oréfice, A.A.R. de Oliveira, M.d.M. Pereira, Synthesis and characterization of biodegradable polyurethane films based on HDI with hydrolyzable crosslinked bonds and a homogeneous structure for biomedical applications, Mater. Sci. Eng: C 52 (2015) 22-30.

[31] S.A. Guelcher, K.M. Gallagher, J.E. Didier, D.B. Klinedinst, J.S. Doctor, A.S. Goldstein, G.L. Wilkes, E.J. Beckman, J.O. Hollinger, Synthesis of biocompatible segmented polyurethanes from aliphatic diisocyanates and diurea diol chain extenders, Acta Biomater. 1(4) (2005) 471-84.

[32] M. Bil, J. Ryszkowska, P. Wo niak, K.J. Kurzydłowski, M. Lewandowska-Szumieł, Optimization of the structure of polyurethanes for bone tissue engineering applications, Acta Biomater. 6(7) (2010) 2501-2510.

[33] Y. Niu, K.C. Chen, T. He, W. Yu, S. Huang, K. Xu, Scaffolds from block polyurethanes based on poly(•-caprolactone) (PCL) and poly(ethylene glycol) (PEG) for peripheral nerve regeneration, Biomaterials 35(14) (2014) 4266-4277.

[34] M. Li, J. Chen, M. Shi, H. Zhang, P.X. Ma, B. Guo, Electroactive anti-oxidant polyurethane elastomers with shape memory property as non-adherent wound dressing to enhance wound healing, Chem. Eng. J. 375 (2019) 121999.

[35] Y. Hong, 19 - Electrospun fibrous polyurethane scaffolds in tissue engineering, in: S.L. Cooper, J. Guan (Eds.), Advances in Polyurethane Biomaterials, Woodhead Publishing 2016, pp. 543-559.

[36] S. Fernando, M. McEnery, S.A. Guelcher, 16 - Polyurethanes for bone tissue engineering, in: S.L. Cooper, J. Guan (Eds.), Advances in Polyurethane Biomaterials, Woodhead Publishing 2016, pp. 481-501.

[37] N. Zanjanizadeh Ezazi, M.-A. Shahbazi, Y.V. Shatalin, E. Nadal, E. Mäkilä, J. Salonen, M. Kemell, A. Correia, J. Hirvonen, H.A. Santos, Conductive vancomycin-loaded mesoporous silica polypyrrole-based scaffolds for bone regeneration, Int. J. Pharm. 536(1) (2018) 241-250.

[38] N. Zanjanizadeh Ezazi, R. Ajdary, A. Correia, E. Makila, Fabrication and Characterization of Drug-Loaded Conductive Poly(glycerol sebacate)/Nanoparticle-Based Composite Patch for Myocardial Infarction Applications, 12(6) (2020) 6899-6909.

[39] S. Brauman, G. Mayorga, J. Heller, Light stability and discoloration of segmented polyether urethanes, Ann. Biomed. Eng. 9(1) (1981) 45-58.

[40] H.K. Lindberg, A. Korpi, T. Santonen, K. Säkkinen, M. Järvelä, J. Tornaeus, N. Ahonen, H. Järventaus, A.-L. Pasanen, C. Rosenberg, Micronuclei, hemoglobin adducts and

respiratory tract irritation in mice after inhalation of toluene diisocyanate (TDI) and 4, 4•-methylenediphenyl diisocyanate (MDI), Mutation Research/Genetic Toxicology and Environmental Mutagenesis 723(1) (2011) 1-10.

[41] G. Li, D. Li, Y. Niu, T. He, K.C. Chen, K. Xu, Alternating block polyurethanes based on PCL and PEG as potential nerve regeneration materials, J. Biomed. Mater. Res. A 102(3) (2014) 685-97.

[42] Z. Ma, Y. Hong, D.M. Nelson, J.E. Pichamuthu, C.E. Leeson, W.R. Wagner, Biodegradable polyurethane ureas with variable polyester or polycarbonate soft segments: Effects of crystallinity, molecular weight, and composition on mechanical properties, Biomacromolecules 12(9) (2011) 3265-3274.

[43] J. Guan, W.R. Wagner, Synthesis, characterization and cytocompatibility of polyurethaneurea elastomers with designed elastase sensitivity, Biomacromolecules 6(5) (2005) 2833-2842.

[44] J. Seppälä, H. Korhonen, R. Hakala, M. Malin, Photocrosslinkable polyesters and poly (ester anhydride) s for biomedical applications, Macromol. Biosci. 11(12) (2011) 1647-1652.

[45] L.H. Sinh, K. Harri, L. Marjo, M. Minna, N.D. Luong, W. Jürgen, W. Torsten, S. Matthias, S. Jukka, Novel photo-curable polyurethane resin for stereolithography, RSC Adv 6(56) (2016) 50706-50709.

[46] B. van Bochove, G. Hannink, P. Buma, D.W. Grijpma, Preparation of Designed Poly(trimethylene carbonate) Meniscus Implants by Stereolithography: Challenges in Stereolithography, Macromol. Biosci. 16(12) (2016) 1853-1863.

[47] K. Wessler, M.H. Nishida, J. da Silva Jr, A.P.T. Pezzin, S.H. Pezzin, Thermal Properties and Morphology of Poly (3-Hydroxybutyrate-co-3-Hydroxyvalerate) with Poly (Caprolactone Triol) Mixtures, Macromolecular Symposia, Wiley Online Library, 2006, pp. 161-165.

[48] Q. Zhang, Y. Liu, K.C. Chen, G. Zhang, X. Shi, H. Chen, Surface biocompatible modification of polyurethane by entrapment of a macromolecular modifier, Colloids Surf. B. Biointerfaces 102 (2013) 354-360.

[49] D. Chattopadhyay, D.C. Webster, Thermal stability and flame retardancy of polyurethanes, Prog. Polym. Sci. 34(10) (2009) 1068-1133.

[50] V. Kupka, L. Vojtova, Z. Fohlerova, J. Jancar, Solvent free synthesis and structural evaluation of polyurethane films based on poly (ethylene glycol) and poly (caprolactone), Express Polym. Lett 10(6) (2016) 479.

[51] X. Kong, G. Liu, J.M. Curtis, Novel polyurethane produced from canola oil based poly (ether ester) polyols: Synthesis, characterization and properties, Eur. Polym. J. 48(12) (2012) 2097-2106.

[52] H. Yeganeh, M.M. Lakouraj, S. Jamshidi, Synthesis and properties of biodegradable elastomeric epoxy modified polyurethanes based on poly (-caprolactone) and poly (ethylene glycol), Eur. Polym. J. 41(10) (2005) 2370-2379.

[53] Z. Hou, J. Xu, J. Teng, Q. Jia, X. Wang, Facile preparation of medical segmented poly (ester-urethane) containing uniformly sized hard segments and phosphorylcholine groups for improved hemocompatibility, Mater. Sci. Eng: C 109 (2020) 110571.

[54] H.-Y. Mi, X. Jing, B.N. Napiwocki, B.S. Hagerty, G. Chen, L.-S. Turng, Biocompatible, degradable thermoplastic polyurethane based on polycaprolactone-block-polytetrahydrofuran-block-polycaprolactone copolymers for soft tissue engineering, J. Mater. Chem B 5(22) (2017) 4137-4151.

[55] H.-Y. Mi, X. Jing, G. Yilmaz, B.S. Hagerty, E. Enriquez, L.-S. Turng, In situ synthesis of polyurethane scaffolds with tunable properties by controlled crosslinking of tri-block copolymer and polycaprolactone triol for tissue regeneration, Chem. Eng. J. 348 (2018) 786-798.

[56] A.M. Coenen, K.V. Bernaerts, J.A. Harings, S. Jockenhoevel, S. Ghazanfari, Elastic materials for tissue engineering applications: Natural, synthetic, and hybrid polymers, Acta Biomater. 79 (2018) 60-82.

[57] W. Zhu, K.R. Tringale, S.A. Woller, S. You, S. Johnson, H. Shen, J. Schimelman, M. Whitney, J. Steinauer, W. Xu, Rapid continuous 3D printing of customizable peripheral nerve guidance conduits, Mater. Today 21(9) (2018) 951-959.

[58] M. Griffin, Y. Premakumar, A. Seifalian, P.E. Butler, M. Szarko, Biomechanical characterization of human soft tissues using indentation and tensile testing, JoVE-J VIS EXP 118 (2016) e54872.

[59] I.P. Herman, Physics of the human body, Springer 2016.

[60] S. Khan, I. Plitz, R. Frantz, In situ technique for monitoring the gelation of UV curable polymers, Rheol. Acta 31(2) (1992) 151-160.

[61] D.P. Dowling, I.S. Miller, M. Ardhaoui, W.M. Gallagher, Effect of surface wettability and topography on the adhesion of osteosarcoma cells on plasma-modified polystyrene, J. Biomater. Appl. 26(3) (2011) 327-347.

[62] C.S. Schollenberger, F.D. Stewart, Thermoplastic polyurethane hydrolysis stability, Die Angewandte Makromolekulare Chemie 29(1) (1973) 413-430.

[63] J.H. Jung, M. Ree, H. Kim, Acid-and base-catalyzed hydrolyses of aliphatic polycarbonates and polyesters, Catal. Today 115(1-4) (2006) 283-287.

[64] F.R. Tay, D.H. Pashley, M.C. Williams, R. Raina, R.J. Loushine, R.N. Weller, W.F. Kimbrough, N.M. King, Susceptibility of a polycaprolactone-based root canal filling material to degradation. I. Alkaline hydrolysis, J. Endod. 31(8) (2005) 593-598.

[65] Y. Hou, J. Chen, P. Sun, Z. Gan, G. Zhang, In situ investigations on enzymatic degradation of poly (•-caprolactone), Polymer 48(21) (2007) 6348-6353.

[66] M.C. Lensen, V.A. Schulte, M. Diez, Cell Adhesion and spreading on an intrinsically anti-adhesive PEG biomaterial, Biomaterials—Physics and Chemistry; Pignatello, PR, Ed.; INTECH Open Access Publisher: Rijeka, Croatia (2011) 397-414.

[67] M. Zhang, T. Desai, M. Ferrari, Proteins and cells on PEG immobilized silicon surfaces, Biomaterials 19(10) (1998) 953-960.

Highlights

- Fast photocuring PUs were synthesized through solvent free method.
- Flexible PU elastomers showed good mechanical properties needed for soft tissue scaffold.
- 3D scaffold with high resolution and complex geometry was fabricated for soft tissue engineering using SLA.
- High biocompatibility on dermal fibroblast cells was obtained using PU/PCL/PEG.
- 3D Printed scaffold showed higher cell attachment compared with casted film.

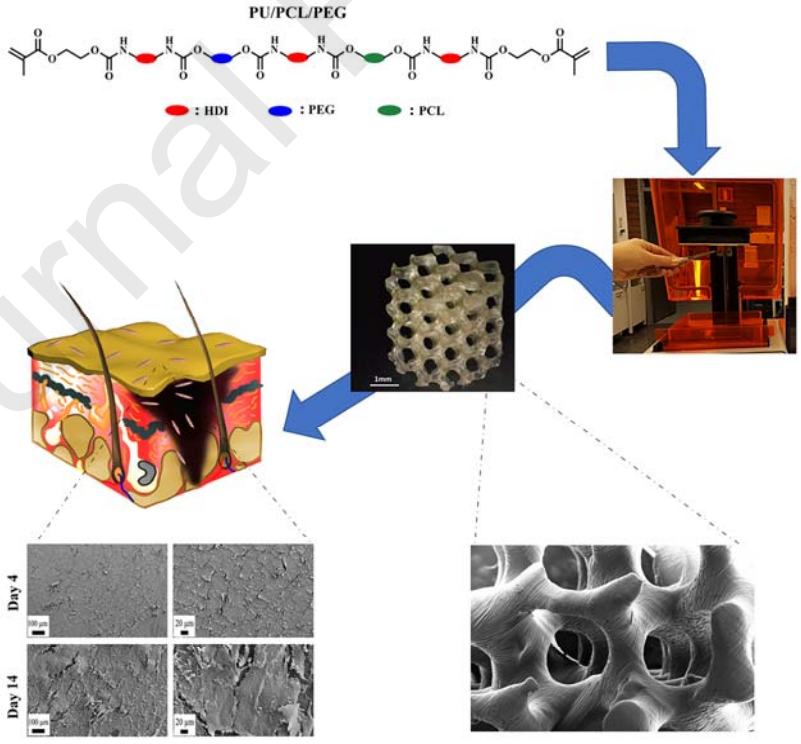

Declaration of interests

☒ The authors declare that they have no known competing financial interests or personal relationships that could have appeared to influence the work reported in this paper.

☐The authors declare the following financial interests/personal relationships which may be considered as potential competing interests:

Author statement

Afsoon Farzan: Conceptualization, Methodology, Validation, Formal analysis, Investigation, Resources, Writing - Original Draft

Sedigheh Borandeh: Conceptualization, Formal analysis, Investigation, Writing - Original Draft, Writing - Review & Editing

Nazanin Zanjanizadeh Ezazi: Methodology, Validation, Resources, Writing - Original Draft

Sami Lipponen: Conceptualization, Review & Editing

Hélder A. Santos: Supervision

Jukka Seppälä: Conceptualization, Supervision